ACS OMEGA

http://pubs.acs.org/journal/acsodf

Article

Synthesis, Characterization, Crystal Structures, and Supramolecular Assembly of Copper Complexes Derived from Nitroterephthalic Acid along with Hirshfeld Surface Analysis and Quantum Chemical Studies

Seadat Suliddin Hasanova, Emina Agil Yolchueva, Aliyeva Qudrat Mashadi, Shabbir Muhammad, Muhammad Ashfaq,* Movsumov Elman Muhammed, Khurram Shahzad Munawar, Muhammad Nawaz Tahir, Abdullah G. Al-Sehemi, and Saleh S. Alarfaji

Cite This: *ACS Omega* 2023, 8, 8530−8540

Read Online

ACCESS | Metrics & More | Article Recommendations | Supporting Information

ABSTRACT: Two new Cu(II) carboxylate complexes, **Cu-NTA** and **Cu-DNTA**, were prepared by treating 2-nitroterephthalic acid with $CuSO_4 \cdot 5H_2O$ at room temperature. The synthesized complexes were characterized by elemental (CHN), FT-IR, and thermogravimetric analysis. The crystal structures of both complexes were explored by single crystal X-ray diffraction analysis, which inferred that the coordination geometry is slightly distorted octahedral and square pyramidal in **Cu-NTA** and **Cu-DNTA**, respectively. The noncovalent interactions that are the main feature of the supramolecular assembly were investigated by Hirshfeld surface analysis for both complexes. The propensity of each pair of chemical moieties involved in crystal-packing interactions was determined by the enrichment ratio. Quantum chemical computations were performed to optimize the molecular geometry of complex **Cu-NTA** and compared it with the experimental single crystal structure, which was found to be in sensible agreement with the experimental structure of the complex. The DFT method was used to see the potential of the selected **Cu-NTA** complex for linear and nonlinear optical properties. The static NLO polarizability <γ> of complex **Cu-NTA** was calculated to be 86.28×10^{-36} esu at M06 functional and 6-31G*/LANL2DZ basis set, which was rationally large to look for NLO applications of complex **Cu-NTA**. Additionally, the molecular electrostatic potential and frontier molecular orbitals were also computed with the same methodology to see electronic characteristics and ground-state electronic charge distributions.

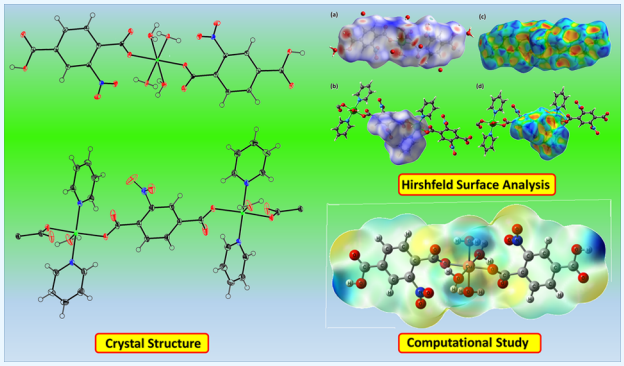

1. INTRODUCTION

Over the past 25 years, a great deal of research has been done on metal complexes based on benzene dicarboxylic acid to better understand their structural characteristics and diverse properties.[1] Dicarboxylates are frequently employed in the construction of coordination polymers with desirable topologies from a synthetic perspective due to their abundant coordination modes and potential to behave like hydrogen bonding acceptors and donors.[2,3] Terephthalic acid, which has two carboxylate groups at the trans position, can be helpful in the preparation of coordination polymers through complete and partial deprotonation due to the evenly spaced carboxylic groups, the stiffness of the phenyl skeleton, and particularly its various bridging modes.[4−6] Additionally, research has demonstrated that the functionalization of the organic linker with either nitro or amino groups can successfully modify the band gap of effective semiconductor supramolecular species.[7] Hence, nitroterephthalic acid is preferred over simple terephthalic acid. There are now more than twenty 2-nitroterephthalic acid complexes that have been identified to have different coordination features.[8−12]

The ability to produce polymers with a larger range of structural characteristics has been made feasible by using mixed ligands rather than a single kind of ligand. As a result, adding auxiliary ligands to the reaction systems, such as aromatic N-donors, can lead to a wide range of structural diversities.[13] The major problem in the process of synthesizing coordination polymers is to control the dimensions. Lower dimensionalities are typically the consequence of the coordination of H_2O or molecules of other solvents by

Received: December 1, 2022
Accepted: February 8, 2023
Published: February 24, 2023

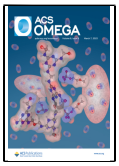

Table 1. SC-XRD Experimental Details of Cu-NTA and Cu-DNTA

crystal parameters	Cu-NTA	Cu-DNTA
chemical formula	$C_{16}H_{16}CuN_2O_{16}$	$C_{18}H_{15}CuN_3O_7$
CCDC	2192298	2192299
M_r	555.86	231.67
crystal system, space group	monoclinic, *I*2/*a*	monoclinic, *C*2/*c*
temperature (K)	100	100
a, *b*, *c* (Å)	18.27331 (13), 6.99598 (5), 15.67276 (12)	15.0291 (13), 5.8680 (5), 21.9408 (18)
α, β, γ (°)	90, 96.6485 (7), 90	90, 104.359 (3), 90
V (Å^3)	1990.13 (3)	1874.5 (3)
Z	4	4
radiation type	Cu K_α	Mo K_α
μ (mm^{-1})	2.438	1.213
crystal size (mm)	0.43 × 0.29 × 0.24	0.25 × 0.20 × 0.03
diffractometer	Bruker Kappa APEXII CCD	Bruker Kappa APEXII CCD
absorption correction	multi-scan (*SADABS*; Bruker, 2007)	multi-scan (*SADABS*; Bruker, 2007)
no. of measured, independent, and observed [$I > 2\sigma(I)$] reflections	8342, 1852, 1848	16,281, 3432, 2427
R_{int}	0.022	0.113
$(\sin \theta/\lambda)_{max}$ (Å^{-1})	0.611	0.759
$R[F^2 > 2\ \sigma(F^2)]$, $wR(F^2)$, *S*	0.025, 0.069, 1.15	0.051, 0.104, 1.05
no. of reflections	1852	3432
no. of parameters	176	150
no. of restraints	8	
H-atom treatment	H-atoms are treated by a mixture of independent and constrained refinement	H-atoms are treated by a mixture of independent and constrained refinement
$\Delta\rho_{max}$, $\Delta\rho_{min}$ (e Å^{-3})	0.34, −0.37	0.53, −0.74

multifunctional ligands that cause steric hindrance around the central metal atoms or ions.[14]

Cueto *et al.* reported that the copper terephthalate trihydrate complex was one of the first metal terephthalate complexes to be described as porous MOFs, and it was further investigated for conductivity and magnetic properties.[15] Mori *et al.* announced the discovery of the first copper terephthalate with a significant surface area.[16,17] It was thought that this first copper terephthalate complex has a paddlewheel-type structure, even though no structural information was ever provided.[18]

Therefore, based on the aforementioned factors and our experience with metal carboxylates,[19−24] in this study, we have described the synthesis of two Cu(II) complexes, **Cu-NTA** and **Cu-DNTA**, from $CuSO_4{\cdot}5H_2O$, nitro-substituted terephthalic acid, and N-donor ligand. The method applied for the synthesis of complexes is very simple, as there is no vigorous heating or reflux needed. The reaction was conducted in aqueous media, which is considered a green and cheap solvent. Additionally, quantum chemical approaches were applied to study the electronic structure and optical and nonlinear optical response properties of the synthesized **Cu-NTA** complex.

2. RESULTS AND DISCUSSION

2.1. SC-XRD Description of Cu-NTA and Cu-DNTA.

The crystal structure of both compounds is determined by the SC-XRD technique. Experimental facts are given in Table 1, whereas important bond lengths (Å) and bond angles (°) are given in Table 2.

In **Cu-NTA** (Figure 1 and Table 1), the asymmetric unit contains half of the molecule, while the remaining half molecule is created by symmetry (i) $-x + 1/2, -y + 5/2, -z + 1/2$. The Cu ion is hexa coordinated using four water molecules and two non-chelating 4-carboxy-2-nitrobenzoate molecules to complete the coordination sphere surrounding the Cu-atom. The bond lengths range from 1.9219 (11) to 2.5164 (11) Å and the bond angles range from 87.34 (5) to 180.0° (Table 2) in the coordination sphere, which indicates that the coordination geometry is slightly distorted octahedral. The phenyl ring A makes the dihedral angles of 41.9 (1), 5.9

Table 2. Important Geometrical Parameters of Cu-NTA and Cu-DNTA[a]

bond lengths (Å) of **Cu-NTA**		bond lengths (Å) of **Cu-DNTA**	
Cu1−O1	1.9754 (11)	Cu1−O1	2.190 (3)
Cu1−O1^{i}	1.9754 (11)	Cu1−O2	1.9754 (16)
Cu1−O2^{i}	2.5164 (11)	Cu1−O2^{ii}	1.9755 (16)
Cu1−O2	2.5164 (11)	Cu1−N1	2.009 (2)
Cu1−O3	1.9219 (11)	Cu1−N1^{ii}	2.009 (2)
Cu1−O3^{i}	1.9219 (11)	O2−C6	1.271 (3)
O3−C1	1.2673 (19)	C7−C9^{iii}	1.386 (3)
selected bond angles (°) of **Cu-NTA**		selected bond angles (°) of **Cu-DNTA**	
O1−Cu1−O1^{i}	180.0	O2−Cu1−O2^{ii}	168.27 (11)
O1−Cu1−O2	91.34 (4)	O2−Cu1−N1	88.61 (7)
O1^{i}−Cu1−O2	88.66 (4)	O2^{ii}−Cu1−N1	91.15 (7)
O3−Cu1−O2	85.72 (4)	O2−Cu1−N1^{ii}	91.15 (7)
O3^{i}−Cu1−O2	94.28 (4)	O2^{ii}−Cu1−N1^{ii}	88.61 (7)
O3−Cu1−O3^{i}	180.0	N1−Cu1−N1^{ii}	177.63 (13)
O3−Cu1−O1	87.34 (5)	O2−Cu1−O1	95.86 (6)
O3^{i}−Cu1−O1	92.66 (5)	O2^{ii}−Cu1−O1	95.86 (6)
O3−Cu1−O1^{i}	92.66 (5)	N1−Cu1−O1	91.18 (7)
O3^{i}−Cu1−O1^{i}	87.34 (5)	N1^{ii}−Cu1−O1	91.18 (7)
Cu1−O1−H1A	108.3 (14)	C8−C7−C9^{iii}	118.3 (2)
Cu1−O1−H1B	108.2 (14)	C9^{iii}−C7−C6	120.4 (2)
H1A−O1−H1B	110.1 (19)	C8−C9−C7^{iii}	120.0 (2)
H2A−O2−H2B	105.6 (19)	C7^{iii}−C9−H9	120.0

[a]Symmetry codes: (i) $-x + 1/2, -y + 5/2, -z + 1/2$; (ii) $-x + 1, y, -z + 1/2$; (iii) $-x + 1, -y + 1, -z$.

https://doi.org/10.1021/acsomega.2c07686
ACS Omega 2023, 8, 8530−8540

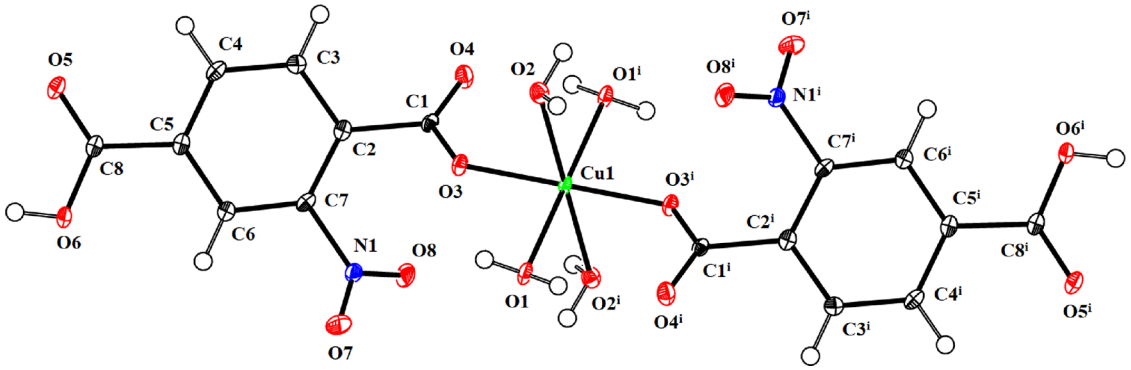

Figure 1. ORTEP diagram of **Cu-NTA** that is drawn at a 50% probability level. The hydrogen atoms are represented as tiny circles with variable radii.

(2), and 47.3 (9)° with the first carboxylate group B (C1/O4/O5), second carboxylate group C (C8/O5/O6), and nitro group C (N1/O7/O8), respectively. The molecules are interconnected to generate dimers *via* O−H···O bonding (Figure S1 and Table 3). The C−H···O bonding, which is comparatively weaker than O−H···O bonding, also plays an important role in crystal packing and interlinking of the dimers. One of the O-atoms of the nitro group behaves like a H-bond acceptor for ortho CH of the benzene ring, whereas the other O-atom of the nitro group is not involved in H-bonding. Two H-atoms of H_2O molecules behave like H-bond donors for the O-atom of the carboxylate group. One of the water molecules also acts as a H-bond acceptor. The packing of the crystal is further stabilized by C−O···π and off-set π···π stacking interactions (Figure 2). The O···π distance for C−O···π interaction is 3.04 Å (Table 3). For off-set π···π stacking interactions, the inter-centroid separation is 3.69 Å (Figure 2) and the ring off-set ranges from 1.483 to 3.520 Å.

Table 3. Hydrogen-Bond Geometry (Å, °) for Cu-NTA and Cu-DNTA Together with *C*−O···π and *C*−O···π Interaction in Cu-NTA and Cu-DNTA, Respectively[a]

Cu-NTA	***D*−H···*A***	***D*−H**	**H···*A***	***D*···*A***	**<(*D*−H···*A*)°**
	O1−H1*A*···O4^{i}	0.83 (2)	1.95 (2)	2.7076 (16)	151 (2)
	O1−H1*B*···O5^{ii}	0.83 (2)	1.91 (2)	2.7315 (16)	169 (2)
	O2−H2*A*···O4^{iii}	0.85 (2)	1.90 (2)	2.7504 (16)	177 (2)
	O2−H2*B*···O6^{iv}	0.84 (2)	2.32 (2)	3.0335 (16)	143 (2)
	O6−H6*A*···O2^{ii}	0.86 (1)	1.85 (1)	2.7005 (16)	177 (2)
	C4−H4···O8^{v}	0.95	2.40	3.278 (2)	154
	***C*−O···π**	**C−O**	**O···π**	***C*···π**	**<(*C*−O···π)°**
	C8−O5···Cg1^{vi}	1.211 (2)	3.0395 (13)	3.3058 (15)	91.73 (9)
Cu-DNTA	***D*−H···*A***	***D*−H**	**H···*A***	***D*···*A***	**<(*D*−H···*A*)°**
	O1−H1*A*···O3^{vii}	0.87 (3)	1.81 (3)	2.673 (3)	172 (4)
	C2−H2···O2^{viii}	0.95	2.57	3.449 (3)	154
	C5−H5···O3^{ix}	0.95	2.60	3.492 (3)	157
	***N*−O···π**	**N−O**	**N···π**	***N*···π**	**<(*N*−O···π)°**
	N2A−O5A···Cg1	1.227 (6)	3.439 (6)	4.419 (5)	137.1 (4)
	N2A−O4A···Cg2^{x}	1.227 (6)	3.502 (4)	4.627 (5)	155.0 (4)

[a]Symmetry codes: (i) − *x* + 1/2, −*y* + 5/2, −*z* + 1/2; (ii) − *x*, −*y* + 2, −*z*; (iii) *x*, *y* + 1, *z*; (iv) *x* + 1/2, −*y* + 2, *z*; (v) x, −y + 1/2 + 1, +z-1/2; (vi) -x,1-y, −z; (vii) − *x* + 1, *y* − 1, −*z* + 1/2; (viii) *x* − 1/2, *y* + 1/2, *z*; (ix) *x*, *y* − 1, *z*; (ix) *x*, *y* + 1, *z*.

The crystal structure of **Cu-DNTA** (Figure 3 and Table 1) is a one-dimensional polymeric compound that extends along the *c*-axis. The central Cu-atom is penta coordinated by the O-atoms of the non-chelating 2-nitroterephthalate ligand, the nitrogen atoms of the pyridine rings, and the O-atom of water. The value of the geometry index τ_5 is calculated to find the exact coordination geometry. The τ_5 value may be zero or one for the square pyramidal and trigonal bipyramidal geometries, respectively. For **Cu-DNTA**, the value of the geometry index is 0.00066, which indicates that the geometry is square pyramidal and the oxygen atom (O1) occupies the axial site. The Cu-atom is deviated by 0.122 Å from the basal plane defined by (N1/N1^{i}/O2/O2^{i}) atoms. The polymer chains are interlinked through O−H···O and moderately weak C−H···O bonding (Figure S2 and Table 3). Both hydrogen atoms of water act as H-donor for one of the oxygen atoms of the carboxylate group. The O-atom of water and the N-atom of the pyridine ring do not play their role as a H-bond acceptor. The packing of the crystal is further stabilized by the N−O···π interaction within a polymeric chain as well as among the polymeric chains (Table 3). One of the O-atoms of the nitro group is involved in the N−O···π interaction within the polymeric chain, whereas the other O-atom of the nitro group is engaged in the N−O···π interaction among the neighboring polymeric chains (Figure S3). In addition to the N−O···π interaction, very weak off-set π···π stacking interactions are present as the inter-centroid separation ranges from 4.8842 (16) to 5.8682 (14) Å.

2.2. Hirshfeld Surface Analysis. Nowadays, the non-covalent interactions in the single crystals can be explored comprehensively with the help of Hirshfeld surface analysis (HSA) using Crystal Explorer version 21.5.[25] The Hirshfeld surface (HS) can be plotted by using various properties like normalized distances (d_{norm}), shape index, etc. The HS plotted over d_{norm} provides the exploration of H-bonding interactions by assigning a different color for short and long contacts. Short contacts are the representatives of the H-bonding interactions.[26−31]

On the HS, the short and long connections are represented by red and blue patches, respectively. The white dots on the HS indicate the connections where the distance between the

https://doi.org/10.1021/acsomega.2c07686
ACS Omega 2023, 8, 8530−8540

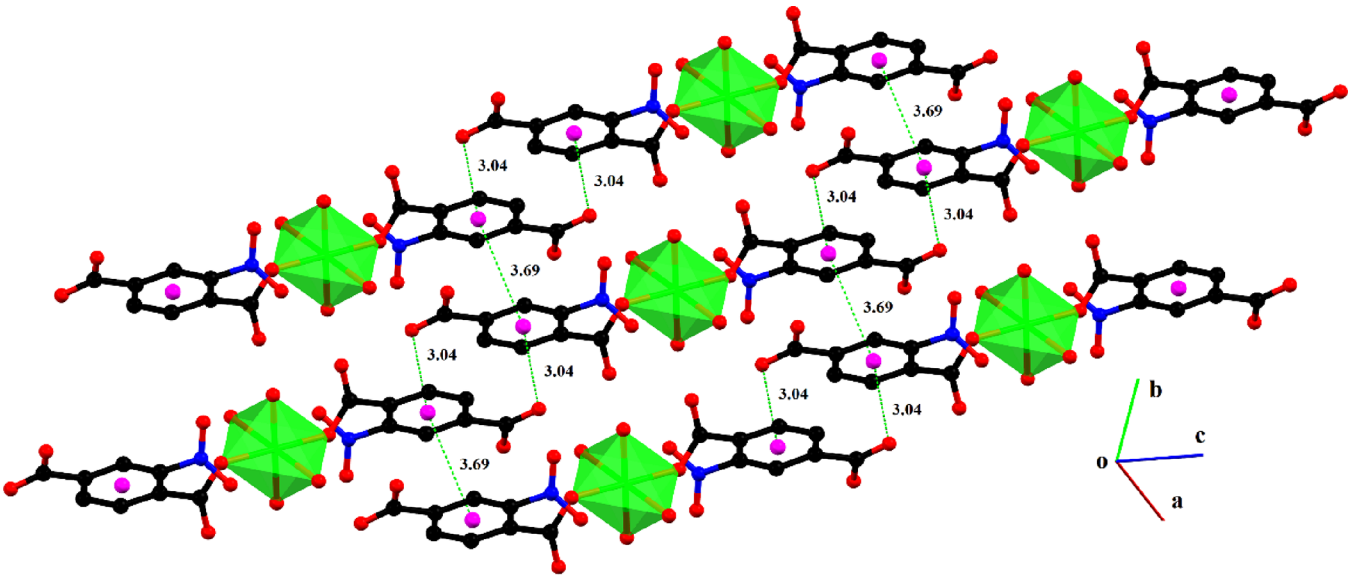

Figure 2. Graphical illustration of C−O···π and off-set π···π stacking interactions. Hydrogen atoms are left out for simplicity. The measurements are given in Å.

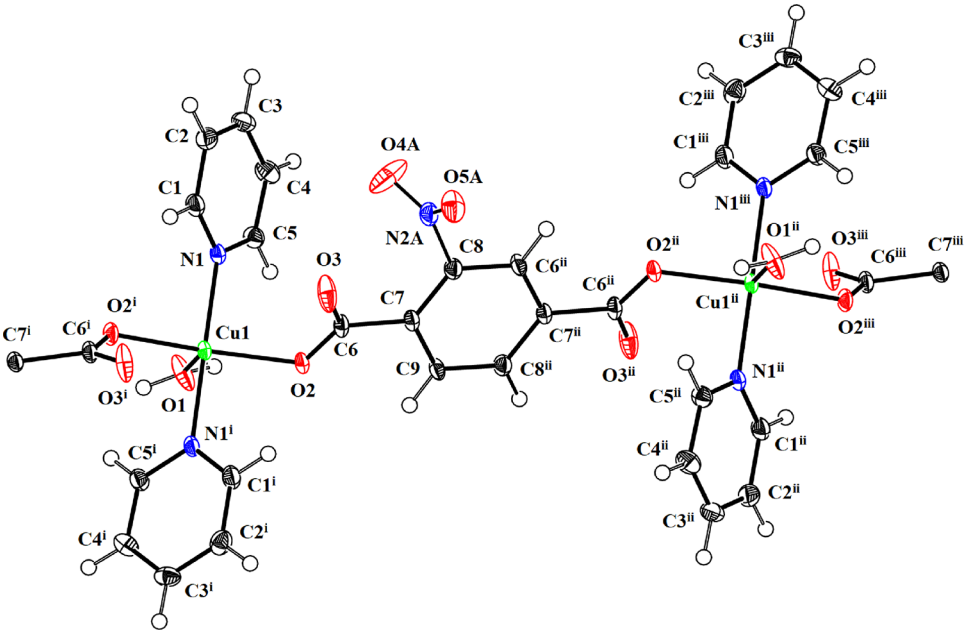

Figure 3. ORTEP diagram of **Cu-DNTA** that is depicted at a 50% probability level. The H-atoms are represented as tiny circles with variable radii. Only the major parts of the disordered nitro group and disordered hydrogen attached to a carbon atom (C8) are shown for clarity.

interacting atoms is smaller than the total of the atoms' van der Waals radii.[32−34] Figure 4a,b shows the HS over d_{norm} for **Cu-NTA** and **Cu-DNTA**, respectively. The red spot on the HS of **Cu-NTA** near carboxylate O-atoms, water molecules, and ortho CH of the benzene ring indicates that these atoms are involved in the H-bonding interactions. For **Cu-DNTA**, only one red spot is found on the HS that is around the Cu-atom, which represents the coordination of the Cu-atom with the symmetry-related O-atom of the 2-nitroterephthalate ligand. The π···π stacking interactions can be visualized by plotting the HS over the shape index. The consecutive red and blue triangular areas around the aromatic ring on the HS plotted over the shape index for **Cu-NTA** (Figure 4c) and **Cu-DNTA** (Figure 4d) designate the existence of π···π stacking interactions in **Cu-NTA** and **Cu-DNTA**.

The short, as well as the comparatively longer, contacts can be quantified by two-dimensional (2D) fingerprint plot analysis.[35−38] 2D fingerprint plots are designed by using the HS as an input. Figure 5a,e shows the 2D plots for the overall interactions for **Cu-NTA** and **Cu-DNTA**, respectively. The central sky blue region represents the π···π stacking interactions, which are larger for **Cu-NTA** (Figure 5a) as compared to **Cu-DNTA** (Figure 5b), which indicates that the π···π stacking interactions are stronger in **Cu-NTA** as compared to **Cu-DNTA**. For both compounds, the most important contacts are O···H, H···H, and C···H, having percentage contributions of 50.9, 18.3, and 5% in **Cu-NTA** and 41.8, 20.5, and 16.5% in **Cu-DNTA**. The remaining 2D fingerprint plots that are comparatively less important are shown in Figures S4 and S5 for **Cu-NTA** and **Cu-DNTA**,

https://doi.org/10.1021/acsomega.2c07686
ACS Omega 2023, 8, 8530−8540

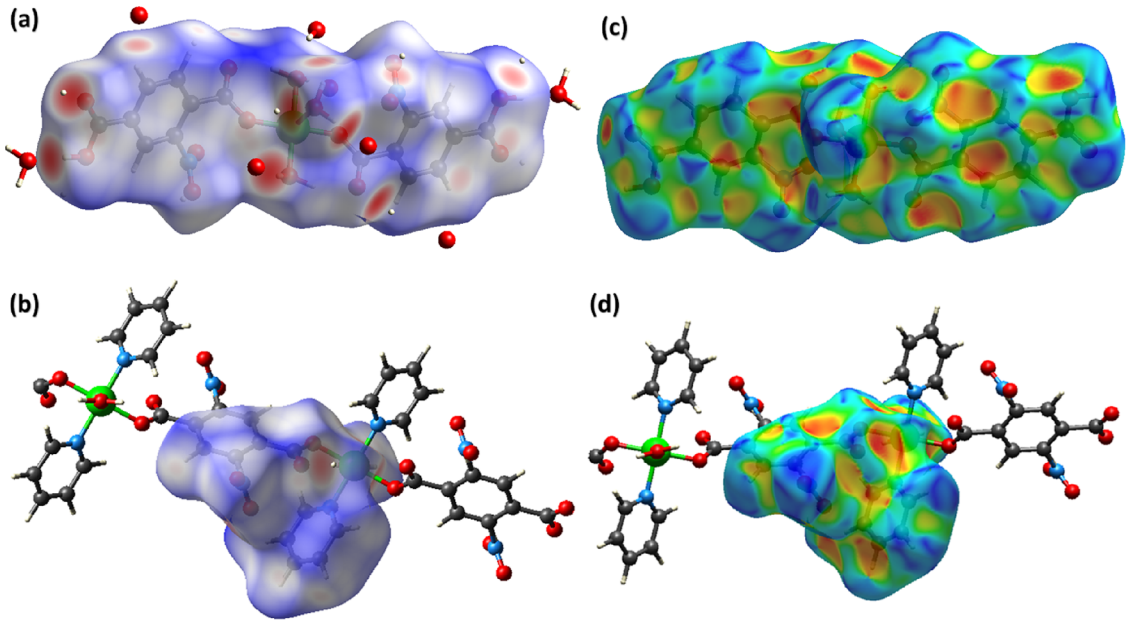

Figure 4. HS plotted over d_{norm} for (a) **Cu-NTA** in the range of −0.6920 to 1.2737 a.u. and (b) **Cu-DNTA** in the array of −1.2743 to 1.1532 a.u. The HS plotted over the shape index in the range of −1 to 1 a.u. for (c) **Cu-NTA** and (d) **Cu-DNTA**.

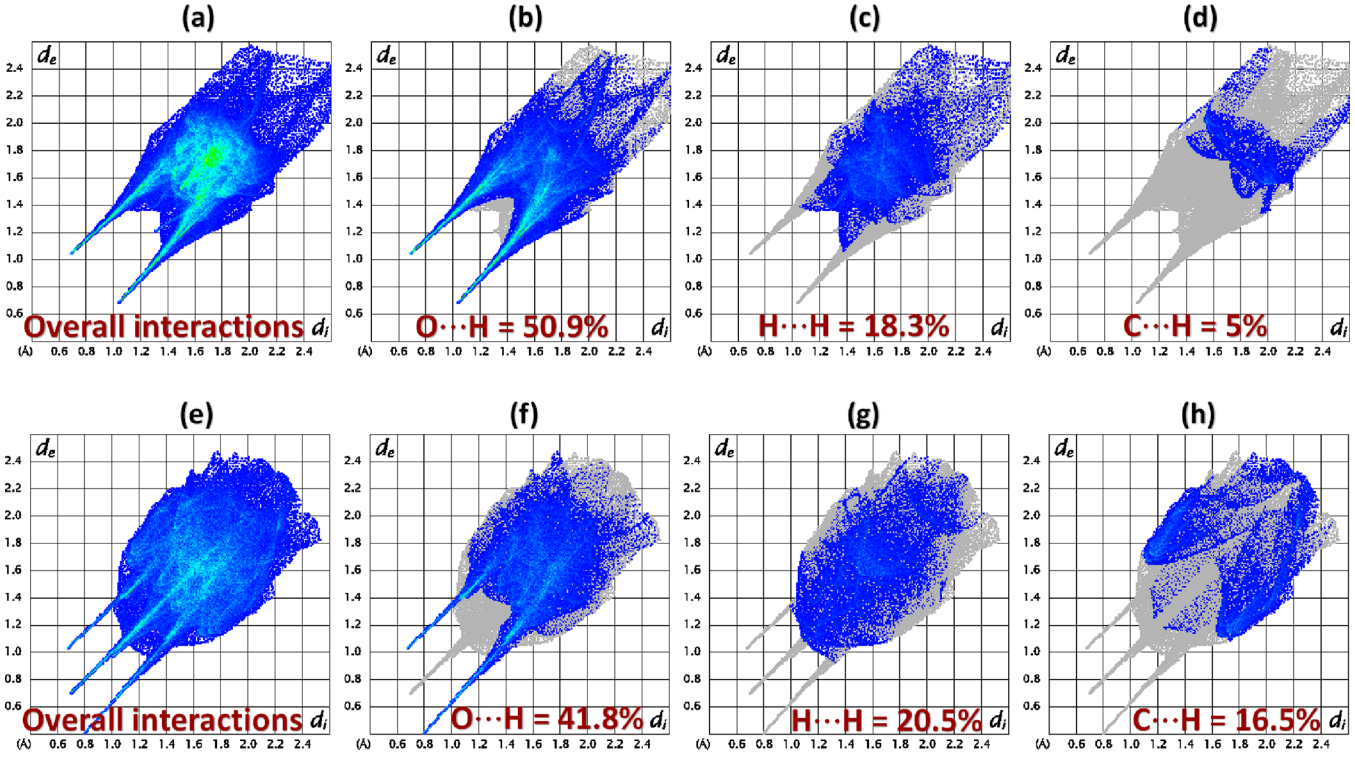

Figure 5. 2D fingerprint plots showing significant interatomic contacts and overall interactions (a–d) for **Cu-NTA** and (e, f) for **Cu-DNTA**.

respectively. The combination of chemical species has a unique tendency for crystal-packing interactions. The propensity of one pair is different from other pairs. The enrichment ratio provides the propensity by dividing the proportion of the actual contacts in the crystal by the theoretical proportion of the random contacts.[39−41] Tables S1 and S2 list the enrichment ratio of the pair of chemical moieties in **Cu-NTA** and **Cu-DNTA**, respectively. The contacts with an enrichment ratio greater than one have a higher propensity to generate crystal-packing interactions relative to other contacts. For both compounds, C···C and O···H contacts have a higher propensity than other contacts, with enrichment ratios of 3.74 and 1.45, respectively, in **Cu-NTA** and 2.28 and 1.53, respectively, in **Cu-DNTA**. C···H contacts have a higher propensity in **Cu-NTA** as compared to **Cu-DNTA**. The N···O contacts have a higher propensity in **Cu-DNTA** as compared to in **Cu-NTA**, which is due to the fact that the N−O···π interaction is present in **Cu-DNTA**, which is absent in **Cu-NTA**.

https://doi.org/10.1021/acsomega.2c07686
ACS Omega 2023, 8, 8530−8540

2.3. Void Analysis. The voids are directly associated with the mechanical properties of the single crystals. If a single crystal has a very small number of voids, then it means that it will have good mechanical properties like a response to applied stress, melting point, etc. From this perspective, we have calculated voids in **Cu-NTA** and **Cu-DNTA** by assuming that all the atoms are spherically symmetric and by adding the electronic density of all the atoms existing in the crystal structure.[42−45] Figure S6 shows the voids present in the crystal packing of **Cu-NTA** and **Cu-DNTA**, respectively. The study inferred that the percentage space occupied by voids is 7.5 and 8.9% in **Cu-NTA** and **Cu-DNTA**, respectively, which indicates that in both compounds, the molecules are strongly packed without significant cavities.

2.4. FT-IR Spectral Investigations. According to the literature,[46] the FT-IR spectra of copper complexes displayed absorption bands in their definite sections. The most noticeable difference was the disappearance of wider bands at 3400 cm^{-1} in the **Cu-DNTA** spectra, which are thought to be due to COOH vibrations of the free ligand. The appearance of additional medium-intensity bands around 550 cm^{-1} for both complexes owing to Cu−O bonding further confirmed the existence of coordinated deprotonated carboxylate ligands in the spectra of the complexes. Asymmetric and symmetric COO^- vibrations in **Cu-NTA** showed prominent bands at 1658 and 1425 cm^{-1}, respectively, with a $\Delta\nu$ value of 233, indicating a monodentate mode of carboxylate ligand binding. The two strong bands were seen for the COO^- moiety's asymmetric (1665 cm^{-1}) and symmetric (1430 cm^{-1}) vibrations in **Cu-DNTA**, with a $\Delta\nu$ value of 235, which also guarantees the monodentate mode of coordination of the carboxylate ligand. The SC-XRD data further confirms the mode of coordination of the ligands. The medium-intensity bands at 650 cm^{-1} due to the newly formed Cu−N bond represent the coordination of pyridine to the copper core in **Cu-DNTA**. The coordinated water molecules show their presence as a broad band from 3300 to 2800 cm^{-1} in both complexes.

2.5. Thermogravimetric Analysis. Thermolysis of both complexes occurs in four stages at different temperature intervals: In the first stage of **Cu-NTA** at a temperature range of 180−200 °C, four H_2O molecules are released, accompanied by a weight loss of 12.95%. In the second stage, at a temperature range of 200−365 °C, thermolysis is stable. Apparently, the monomeric structure becomes dimeric, which is characteristic of Cu(II) complexes with benzoic acid derivatives. In the third stage, at 370−495 °C, the breakdown of dimeric molecules occurs, along with the burning out of carbon hydrate residues with a deep exo-effect. In the fourth stage, Cu(II) carbonate is formed (690 °C) and finally decomposes to metal oxides at 780 °C.

In the first stage of **Cu-DNTA** at a temperature range of 175−210 °C, coordinating one molecule of water and two molecules of pyridine are released. The remaining three stages of thermolysis proceeded in the same manner as that of **Cu-NTA**.

3. COMPUTATIONAL RESULTS

3.1. Computational Methodology. Computational calculations were carried out using the Gaussian 16 program[47] to understand the **Cu-NTA** complex's electronic properties. The initial geometry of the **Cu-NTA** complex, which served as the starting configuration for the search for optimal geometry, was taken from the crystal structure. The optimization of the molecular structure was conducted with the help of the M06 method with a mixed basis set of 6-31G*/LanL2DZ. In some prior studies, the reliability of the Minnesota family functionals (M06 and M06-2X) has been evaluated and found to be better than other currently available conventional DFT functionals.[48,49] For theoretical calculations of transition metal complexes, LanL2DZ relativistic pseudopotentials have proven to be more trustworthy and yield findings that are equivalent to experimental data. Both of these basis sets were applied to different atoms of the complex, as LanL2DZ was utilized for Cu metal and 6-31G* was for carbon, oxygen, nitrogen, and hydrogen. The calculations of dipole moment, linear polarizability, and third-order nonlinear polarizability of the **Cu-NTA** complex were performed by using the same level of theory. The GaussView 6.0.16[50] was used to analyze the complex's ground-state optimal geometry, frontier molecular orbital energy profile, and three-dimensional molecular electrostatic potential map. Further computational details can be seen in our previously published full computational studies papers.[51−54]

The dipole moment (μ) and linear polarizability ($\alpha_\circ$) can be calculated by using eqs 1 and 2:

$$\mu = (\mu_x^2 + \mu_y^2 + \mu_z^2) \tag{1}$$

$$\alpha_\circ = \frac{1}{3}(\alpha_{xx} + \alpha_{yy} + \alpha_{zz}) \tag{2}$$

The second hyperpolarizability is calculated by using eq 3:

$$\langle\gamma\rangle = \frac{1}{15}\sum_{ij=x,y,z}(\gamma_{iijj} + \gamma_{ijij} + \gamma_{ijji}) \tag{3}$$

These tensors are reduced to only six components (by Kleinman symmetry) using eq 4:

$$\langle\gamma\rangle = \frac{1}{15}(\gamma_{xxxx} + \gamma_{yyyy} + \gamma_{zzzz} + 2(\gamma_{xxyy} + \gamma_{xxzz} + \gamma_{yyzz})) \tag{4}$$

3.2. Computational Geometry Optimization for the Cu-NTA Complex. Nowadays, computational calculations are commonly used to describe the structural properties of many compounds. Among the above-synthesized compounds, we chose the **Cu-NTA** complex for studying its geometry and other electronic properties through computational tools because the molecular geometry of the **Cu-DNTA** complex has not been obtained due to its larger size and involvement of multiple metal atoms. The geometry optimization of the **Cu-NTA** complex has been carried out by employing the M06 functional. For comparison of geometrical parameters, experimentally (within parenthesis) and theoretically (without parentheses) observed bond lengths of the **Cu-NTA** complex are shown in Figure S7. The **Cu-NTA** complex consists of two ligands of 2-nitroterephthalic acid (**NTA**) and four solvent water molecules bound to the Cu(II) ion in an octahedral coordination environment. Cu(II) ion occupies a centrosymmetric inversion center. Two ligands of 2-nitroterephthalic acid occupy two trans axial positions in this coordination environment. In the equatorial plane, the Cu1−O33 and Cu1−O8 (oxygen atom of 2-nitroterephthalic acid) bond distance is 1.921 Å in the crystal structure and 1.938 Å in the calculated structure. A noticeable difference is observed between the crystal structure and theoretical bond lengths in

https://doi.org/10.1021/acsomega.2c07686
ACS Omega 2023, 8, 8530−8540

the two axial bonds of Cu1−O2 and Cu1−O27. That is 1.975 Å experimentally, while it is appreciably elongated to 2.141 Å in computed geometry. The long bonds of Cu, including Cu1−O30 and Cu−O5, are seen at 2.516 Å in the XRD structure for a d^9 system of Cu, while it is reduced to 2.234 Å in an optimized structure. Possible causes of this bond length reduction include phase changes because the XRD structure is analyzed in the solid phase and theoretical calculations are performed in the gas phase. There are no catastrophic disagreements between the experimental and theoretical bond distances among 2-nitroterephthalic acids, as manifested in Figure S7. This comparison offers confidence that the M06 functional can be used for further calculations.

3.3. Linear and Third-Order NLO Properties. Nonlinear optical materials play a vital role in recent technology development. The NLO materials are utilized in laser frequency doubling, telecommunication, and other digital data storage and processing. The third-order NLO response has been calculated through the calculation of second hyperpolarizability (gamma) amplitudes. Besides this, linear polarizability, which shows a linear response to the applied electric field, has also been calculated at the same level of theory. Linear polarizability also plays a key role while designing electro-optical materials. Table S3 shows the amplitudes of linear polarizability and third-order NLO polarizability with their individual components. The isotropic and anisotropic linear polarizabilities are calculated to be 41.23 × 10^{-24} and 41.03 × 10^{-24} esu, respectively. The nonzero polarizability shows the tendency of the molecules to polarize their electric cloud under an applied electric field. The isotropic and anisotropic amplitudes are similar, which indicates that there are no directional aspects and the molecule shows similar polarization regardless of its orientation.

Most importantly, the static <γ> amplitude of **Cu-NTA** is seen to be 86.28 × 10^{-36} esu. Besides this, we have also calculated the frequency-dependent second hyperpolarizability in the form of $\gamma(-w;w,0,0)$ and $\gamma(-2w;w,w,0)$ with an applied wavelength of 1060 nm. The frequency-dependent values of $\gamma(-w;w,0,0)$ and $\gamma(-2w;w,w,0)$ are found to be 118.56 × 10^{-36} and 256.49 × 10^{-36} esu, which are larger than the static values of the second hyperpolarizability. The calculated third-order NLO amplitudes are found to be reasonably large and also comparable to some previously reported metal complexes,[55−57] which show its potential to consider **Cu-NTA** a fair contender for NLO applications.

3.4. Frontier Molecular Orbital and Molecular Electrostatic Potential Diagram. The frontier molecular orbitals, which include HOMO−LUMO, serve as an example of the chemical reactivity and kinetic stability of the molecules. Figure 6 shows the frontier molecular orbital surfaces to better understand the bonding structure of the **Cu-NTA** complex. The highest occupied molecular orbital (HOMO) distribution indicates that the charge density is evenly distributed over the metal and its ligands. In distinction, the electronic density in the lowest unoccupied molecular orbital (LUMO) is concentrated on the **NTA** ligands exclusively. The electronic density transfers from the occupied d orbitals of the metals to the unoccupied antibonding π orbital of the ligand. The energy gap between HOMO and LUMO in **Cu-NTA** is 5.14 eV, showing its polarizability and higher chemical reactivity with lower kinetic stability.

The molecular electrostatic potential (MEP) postulates the nucleophilic and electrophilic sites over the total density

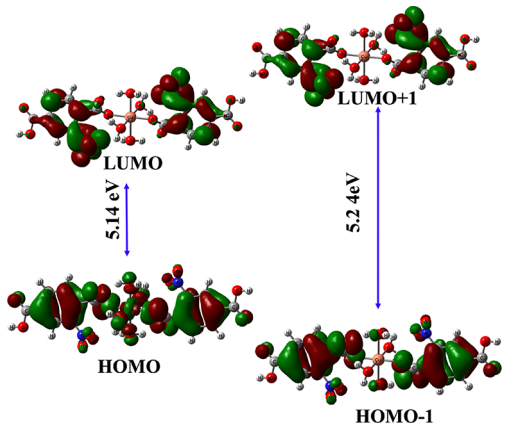

Figure 6. Frontier molecular orbitals of the **Cu-NTA** complex calculated at the M06 functional.

surface of a complex.[58−60] The MEP of the **Cu-NTA** complex is exhibited in Figure 7. A positive electrostatic potential is present at both ends of the **NTA** ligands on the oxygen atom attached to hydrogen in the carboxylic group, which is shown by the blue color. It provides a site for nucleophilic attack. It might be caused by a drop in electron density because electron density moves toward the doubly bounded oxygen atom of the carboxylic group indicated by the yellow color providing a site for electrophilic attack. Moreover, the yellow color is also present on the oxygen atom of the carboxylate group in the **NTA** ligand other than the oxygen that is linked to copper metal because the electron density of the double bond moves toward this oxygen and electrons in the d orbital of Cu metal transfer toward another oxygen atom. The oxygen atom of water molecules that are attached to Cu metal represents a slight blue color related to nucleophilic reactivity.

4. CONCLUSIONS AND PERSPECTIVES

The current research work presents the synthesis, crystal structure, spectroscopic characterization, and computational studies of two copper complexes derived from nitroterephthalic acid. The synthetic procedure is very simple and produces the complexes in a pure form with excellent yield. The SC-XRD study inferred that the coordination geometry is relatively different in **Cu-NTA** and **Cu-DNTA**. The HSA concludes that O···H, H···H, and C···H contacts have a higher contribution in the crystal packing as compared to other contacts, but C···H contacts have a higher propensity to form the crystal-packing interaction in **Cu-NTA** as compared to **Cu-DNTA.** The DFT method is used to study the selected **Cu-NTA** complex for its linear and nonlinear optical properties. The molecular geometry of complex **Cu-NTA** is optimized by quantum chemical computations and compared with its experimental single crystal structure, which is found to be in sensible agreement with the experimental structure of the complex. The static NLO polarizability <γ> of complex **Cu-NTA** is found to be 86.28 × 10^{-36} esu at the M06 functional and 6-31G*/LAN2DZ basis set. Additionally, we have also calculated the frequency-dependent second hyperpolarizability in the form of $\gamma(-w;w,0,0)$ and $\gamma(-2w;w,w,0)$ with an applied wavelength of 1060 nm. The frequency-dependent values of $\gamma(-w;w,0,0)$ and $\gamma(-2w;w,w,0)$ are found to be 118.56 × 10^{-36} and 256.49 × 10^{-36} esu, which are larger than the static γ amplitude. The calculated third-order NLO amplitudes are found to be reasonably large to consider **Cu-NTA** a fair

https://doi.org/10.1021/acsomega.2c07686
ACS Omega 2023, 8, 8530−8540

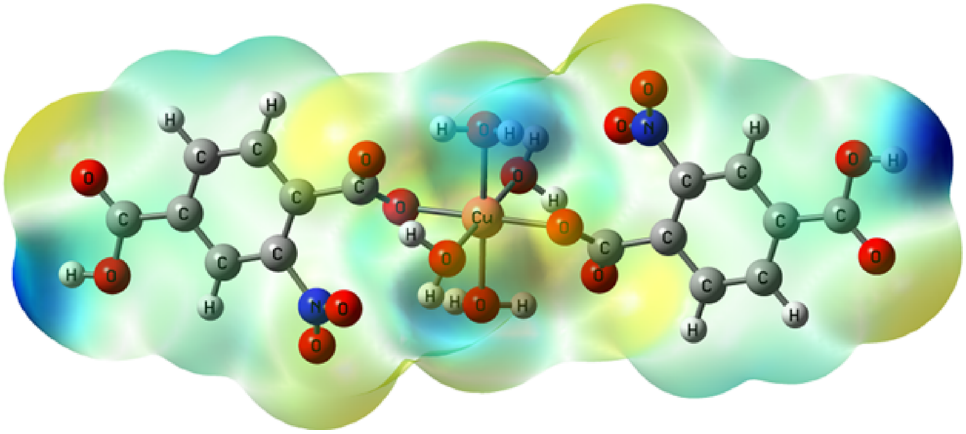

Figure 7. MEP diagram of the **Cu-NTA** complex, where the iso-surface value is 0.002 a.u. The blue and red colors indicate the positive and negative potential maxima, respectively.

contender for NLO applications. Moreover, the MEP and frontier molecular orbital are also computed with the same methodology to see electronic characteristics and ground-state electronic charge distributions.

5. EXPERIMENTAL SECTION

5.1. Materials and Methods. The analytical-grade compounds that are readily available commercially are employed in the current research work. The infrared spectra from 450 to 4000 cm^{-1} were measured using KBr pellets with a PerkinElmer Spectrum 100 FT-IR spectrophotometer. The NETZSCH STA-409 PC/PG derivatograph was used for thermal analysis. The DTA, TG, and DTG curves were measured at an increasing heating rate of 10 °C per min from ambient to 800 °C with the help of platinum crucibles under nitrogen atmosphere. The Costech ECS 4010 CHNSO analyzer was used for elemental analysis (CHN).

5.2. Synthesis of Cu-NTA. The Cu(II) complex (**Cu-NTA**) was prepared by dissolving 2.11 g (10 mmol) of 2-nitroterephthalic acid in 25 mL of hot distilled water, to which an aqueous solution (25 mL) of 1.25 g (5 mmol) of $CuSO_4 \cdot 5H_2O$ was added with continuous stirring and then left at room temperature (Scheme 1). After a few days, bluish-colored prismatic crystals settled down. The crystals were filtered and dried in a desiccator under anhydrous conditions to a constant weight.

Cu-NTA: Yield 81%; **Color** Blue; Anal. Calcd for $C_{16}H_{16}CuN_2O_{16}$ (%): C, 34.57; H, 2.90; N, 5.04. **Found** %: C, 34.65; H, 2.86; N, 4.98; FT-IR (cm^{-1}): 1658s $\nu(COO)_{asym}$, 1425s $\nu(COO)_{sym}$, 233 = $\Delta\nu$, 1365s ν(C=C), 690s ν(C−NO_2), 550s ν(Cu−O), 3400b ν(Cu−H_2O).

5.3. Synthesis of Cu-DNTA. 2-Nitroterephthalic acid 2.11 g (10 mmol) was dissolved in 25 mL of hot distilled water, to which an aqueous solution (25 mL) of 1.68 g (20 mmol) of $NaHCO_3$ was added drop by drop with continuous stirring. Then, an aqueous solution (25 mL) of 2.50 g (10 mmol) of $CuSO_4 \cdot 5H_2O$ was added to it (Scheme 1). After that, 2−3 drops of pyridine were added and the flask containing the reaction mixture was left as such for a few days until the blue needle-like crystals of **Cu-DNTA** appeared. The resulting crystals were filtered and dried in a desiccator over anhydrous $CaCl_2$.

Cu-DNTA: Yield 80%; **Color** Blue; Anal. Calcd for $C_{18}H_{15}CuN_3O_7$ (%): C, 48.16; H, 3.37; N, 9.36. **Found** %: C, 48.13; H, 3.35; N, 9.38; FT-IR (cm^{-1}): 1665s $\nu(COO)_{asym}$, 1430s $\nu(COO)_{sym}$, 235 = $\Delta\nu$, 1367s ν(C=C), 692s ν(C−NO_2), 650s ν(Cu−N), 551s ν(Cu−O).

Scheme 1. Synthesis of Cu-NTA and Cu-DNTA

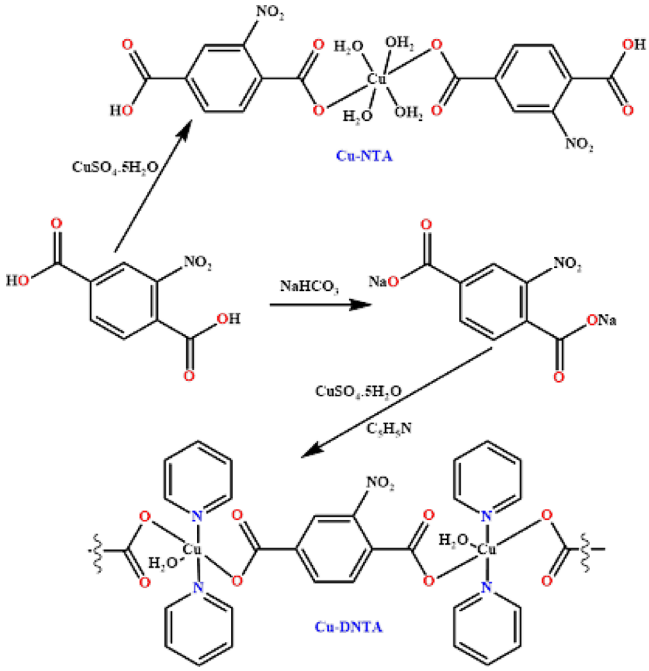

5.4. Single Crystal X-ray Diffraction Procedure. The single crystal XRD data of both complexes were collected on a Bruker Kappa Apex-II CCD diffractometer having APEX-II software. The structure solution is performed on SHELXT-2014[61] and structure refinement is done on SHELXL 2019/2.[62] All non-hydrogen atoms are refined with the help of anisotropic displacement parameters, while hydrogen atoms are assigned by isotropic displacement parameters. All H-atoms are added in the refinement model by using the riding model except the H-atoms attached to O-atoms (O1/O2/O6) in the case of **Cu-NTA** and O-atom (O1) in the case of **Cu-DNTA**. The H-atoms attached to the above-mentioned O-atoms are refined freely for finding the correct orientation of these H-atoms. ORTEP-III,[63] PLATON,[64] and Mercury 4.0[65] are used for graphical illustrations.

https://doi.org/10.1021/acsomega.2c07686
ACS Omega 2023, 8, 8530−8540

■ ASSOCIATED CONTENT

Supporting Information

The Supporting Information is available free of charge at https://pubs.acs.org/doi/10.1021/acsomega.2c07686.

Figure S1: Packing diagram of Cu-NTA. Selected H-atoms are shown for clarity. Figure S2: Packing diagram of Cu-DNTA. Selected H-atoms are shown for clarity. Figure S3: Graphical representation of the N−O···π interaction in Cu-DNTA. Hydrogen atoms are omitted for clearness. Figure S4: Remaining 2D fingerprint plots of Cu-NTA. Figure S5: Remaining 2D fingerprint plots of Cu-DNTA. Figure S6. Graphical representation of voids in the crystal packing of (a) Cu-NTA and (b) Cu-DNTA. Figure S7. The geometrical comparison of experimental and calculated structures of Cu-NTA at the M06 functional. The values in parenthesis are from experimental single crystal data. Table S1. Enrichment ratio for the pair of chemical moieties in Cu-NTA. Table S2. Enrichment ratio for the pair of chemical moieties in Cu-DNTA. Table S3. The computed amplitudes of linear polarizability (α × 10−24) and NLO hyperpolarizability (γ × 10−36) for compound Cu-NTA (PDF)

■ AUTHOR INFORMATION

Corresponding Author

Muhammad Ashfaq − *Department of Physics, University of Sargodha, Sargodha 40100, Pakistan;* orcid.org/0000-0001-6663-8777; Email: ashfaq.muhammad@uos.edu.pk, muhammadashfaq1400@gmail.com

Authors

Seadat Suliddin Hasanova − *Azerbaijan State Agrarian University, Ganja 2000, Azerbaijan*

Emina Agil Yolchueva − *Azerbaijan State Agrarian University, Ganja 2000, Azerbaijan*

Aliyeva Qudrat Mashadi − *Institute of Catalysis and Inorganic Chemistry, Azerbaijan National Academy of Sciences, Baku AZ1143, Azerbaijan*

Shabbir Muhammad − *Department of Chemistry, College of Science, King Khalid University, Abha 61413, Saudi Arabia;* orcid.org/0000-0003-4908-3313

Movsumov Elman Muhammed − *Azerbaijan State Agrarian University, Ganja 2000, Azerbaijan*

Khurram Shahzad Munawar − *Institute of Chemistry, University of Sargodha, Sargodha 40100, Pakistan;* Present Address: Present address: Department of Chemistry, University of Mianwali, Mianwali 42200, Pakistan; orcid.org/0000-0001-9055-2519

Muhammad Nawaz Tahir − *Department of Physics, University of Sargodha, Sargodha 40100, Pakistan;* orcid.org/0000-0002-6815-9806

Abdullah G. Al-Sehemi − *Department of Chemistry, College of Science, King Khalid University, Abha 61413, Saudi Arabia;* orcid.org/0000-0002-6793-3038

Saleh S. Alarfaji − *Department of Chemistry, College of Science, King Khalid University, Abha 61413, Saudi Arabia;* orcid.org/0000-0001-7297-7185

Complete contact information is available at: https://pubs.acs.org/10.1021/acsomega.2c07686

Notes

The authors declare no competing financial interest.

■ ACKNOWLEDGMENTS

The authors from King Khalid University extend their appreciation to the Ministry of Education in KSA for funding the research work through project number KKU-IFP2-DB-7.

■ REFERENCES

(1) Jyai, R. N.; Srinivasan, B. R. Syntheses, structures, reactivity studies and properties of anionic water rich bivalent metal phthalates. *J. Mol. Struct.* **2019**, *1178*, 89−99.

(2) Yang, Y. Y.; Zhou, L.-X.; Zheng, Y. Q.; Zhu, H.-L.; Li, W.-Y. Hydrothermal synthesis, photoluminescence and photocatalytic properties of two silver (I) complexes. *J. Solid State Chem.* **2017**, *253*, 211−218.

(3) Hussain, S.; Ali, S.; Shahzadi, S.; Tahir, M. N.; Shahid, M.; Munawar, K. S.; Abbas, S. M. Synthesis, spectroscopy, single crystal XRD and biological studies of multinuclear organotin dicarboxylates. *Polyhedron* **2016**, *117*, 64−72.

(4) Sun, D.; Zhang, N.; Huang, R.-B.; Zheng, L.-S. Series of Ag (I) coordination complexes derived from aminopyrimidyl ligands and dicarboxylates: syntheses, crystal structures, and properties. *Cryst. Growth Des.* **2010**, *10*, 3699−3709.

(5) Zhao, X.; Bu, X.; Nguyen, E. T.; Zhai, Q.-G.; Mao, C.; Feng, P. Multivariable modular design of pore space partition. *J. Am. Chem. Soc.* **2016**, *138*, 15102−15105.

(6) Huan, D.-H.; Zhao, Y.-Q.; Dong, G.-Y.; Yin, F.-J.; Wang, S.-C. Synthesis, crystal structures and photocatalytic properties of four silver (I) coordination polymers based on semirigid bis (pyrazole) and carboxylic acid co-ligands. *Transition Met. Chem.* **2016**, *41*, 701−712.

(7) Usman, M.; Mendiratta, S.; Lu, K. L. Semiconductor metal−organic frameworks: future low-bandgap materials. *Adv. Mater.* **2017**, *29*, 1605071.

(8) Shi, J.; Yin, H.; Zhang, X.; Wu, C. Synthesis and crystal structure of one-dimensional cadmium (II) coordination polymer: [Cd-2(DTB)(Bpy)(2)(H2O)(2)](n) (DTB= 1, 4-dinitro-2, 3, 5, 6-tetracarboxylatebenzene tetravalent anion; Bpy= 2,2′-bipyridyl). *Chin. J. Struct. Chem.* **2004**, *23*, 1266−1268.

(9) Li, H.-M.; Yuan, H.-B.; Yang, S.-Y.; Huang, R.-B. Poly [[[aqua (2, 2′-bipyridine-κN, N′) zinc (II)]-μ-2-nitroterephthalato-κO: O] monohydrate]. *Acta Crystallogr. E: Crystallogr. Commun.* **2010**, *66*, m983−m984.

(10) He, H.-Y.; Zhu, L.-G.; Ng, S. W. catena-Poly[[[[mu]-4,4′-bipyridine-bis[aquacopper(II)]]-di-[mu]-2-nitroterephthalato]]. *Acta Crystallogr. E: Crystallogr. Commun.* **2005**, *61*, m601−m602.

(11) Liu, W.; Shi, J. Synthesis, crystal structure and magnetic behavior of a two-dimensional cobalt (II) complex with benzene-1, 4-dinitro-2, 3, 5, 6-tetracarboxylate tetravalent anion as bridging ligand. *Pol. J. Chem.* **2004**, *78*, 997−1002.

(12) Ma, A.-Q.; Zhu, L.-G.; Ng, S. W. Poly[[[(2,2′-bipyridine)-copper(II)]-hemi-[mu]2-2-nitroterephthalato-hemi-[mu]4-2-nitroterephthalato] monohydrate]. *Acta Crystallogr. E: Crystallogr. Commun.* **2005**, *61*, m483−m484.

(13) Wang, X.-L.; Bi, Y.-F.; Liu, G.-C.; Lin, H.-Y.; Hu, T.-L.; Bu, X.-H. Zn (ii) coordination architectures with mixed ligands of dipyrido [3, 2-d: 2′, 3′-f] quinoxaline/2, 3-di-2-pyridylquinoxaline and benzenedicarboxylate: syntheses, crystal structures, and photoluminescence properties. *CrystEngComm* **2008**, *10*, 349−356.

(14) Abbasi, A.; Tarighi, S.; Badiei, A. A three-dimensional highly stable cobalt (II) metal−organic framework based on terephthalic acid: synthesis, crystal structure, thermal and physical properties. *Transition Met. Chem.* **2012**, *37*, 679−685.

(15) Cueto, S.; Rys, P.; Rys, F. S.; Sanjinez, R.; Straumann, H. P. Electrical and magnetic properties of new copper arylcarboxylates. *J. Magn. Magn. Mater.* **1992**, *104*, 1096−1097.

(16) Mori, W.; Inoue, F.; Yoshida, K.; Nakayama, H.; Takamizawa, S.; Kishita, M. Synthesis of new adsorbent copper (II) terephthalate. *Chem. Lett.* **1997**, *26*, 1219−1220.
(17) Seki, K.; Takamizawa, S.; Mori, W. Characterization of microporous copper (II) dicarboxylates (fumarate, terephthalate, and trans-1, 4-cyclohexanedicarboxylate) by gas adsorption. *Chem. Lett.* **2001**, *30*, 122−123.
(18) Carson, C. G.; Hardcastle, K.; Schwartz, J.; Liu, X.; Hoffmann, C.; Gerhardt, R. A.; Tannenbaum, R., *Synthesis and structure characterization of copper terephthalate metal−organic frameworks*. Wiley Online Library: 2009.
(19) Hafeez, S. T.; Ali, S.; Tahir, M. N.; Iqbal, M.; Munawar, K. S. One-pot synthesis, structural elucidation, DNA binding and alkaline phosphatase inhibition studies of zinc (II) complexes with 4-nitrocinnamic acid and ethylenediamine. *J. Coord. Chem.* **2014**, *67*, 2479−2495.
(20) Ali, N.; Tahir, M. N.; Ali, S.; Iqbal, M.; Munawar, K. S.; Perveen, S. Synthesis, characterization, crystal structures, enzyme inhibition, DNA binding, and electrochemical studies of zinc (II) complexes. *J. Coord. Chem.* **2014**, *67*, 1290−1308.
(21) Hussain, S.; Bukhari, I. H.; Ali, S.; Shahzadi, S.; Shahid, M.; Munawar, K. S. Synthesis and spectroscopic and thermogravimetric characterization of heterobimetallic complexes with Sn (IV) and Pd (II); DNA binding, alkaline phosphatase inhibition and biological activity studies. *J. Coord. Chem.* **2015**, *68*, 662−677.
(22) Javed, F.; Ali, S.; Shahzadi, S.; Sharma, S.; Qanungo, K.; Munawar, K.; Khan, I. Synthesis, characterization, and biological activity of organotin (IV) complexes with 4-oxo-4-[3-(trifluoromethyl) phenylamino] butanoic acid. *Russ. J. Gen. Chem.* **2017**, *87*, 2409−2420.
(23) Raza, H.; Yasmeen, F.; Sarfraz, M.; Salman Habib, M.; Ba-Shammakh, M.; Munawar, K. S.; Ahmad, N. Carbon capture via novel Cu(II)-DDA metal−organic frameworks-based hybrid membranes. *J. Appl. Polym. Sci.* **2022**, *139*, 52309.
(24) Ali, K. S.; Ashfaq, M.; Tahir, M. N.; Movsumov, E. M.; Munawar, K. S. Synthesis, crystal structure, Hirshfeld surface and void analysis of bis(u_2-4-aminobenzoato-k^2O:O')bis[bis(4-aminobenzoato-k^2O,O')diaquathulium(III)] dihydrate. *Acta Crystallogr. E: Crystallogr. Commun.* **2022**, *78*, 282−286.
(25) Spackman, P. R.; Turner, M. J.; McKinnon, J. J.; Wolff, S. K.; Grimwood, D. J.; Jayatilaka, D.; Spackman, M. A. CrystalExplorer: A program for Hirshfeld surface analysis, visualization and quantitative analysis of molecular crystals. *J. Appl. Crystallogr.* **2021**, *54*, 1006−1011.
(26) Spackman, M. A.; Jayatilaka, D. Hirshfeld surface analysis. *CrystEngComm* **2009**, *11*, 19−32.
(27) Khan, B. A.; Hamdani, S. S.; Ahmed, M. N.; Hameed, S.; Ashfaq, M.; Shawky, A. M.; Ibrahim, M. A.; Sidhom, P. A. Synthesis, X-ray diffraction analysis, quantum chemical studies and α-amylase inhibition of probenecid derived S-alkylphthalimide-oxadiazole-benzenesulfonamide hybrids. *J. Enzyme Inhib. Med. Chem.* **2022**, *37*, 1464−1478.
(28) Ashfaq, M.; Ali, A.; Tahir, M. N.; Khalid, M.; Assiri, M. A.; Imran, M.; Munawar, K. S.; Habiba, U. Synthetic Approach to Achieve Halo Imine Units: Solid-State Assembly, DFT Based Electronic and Non Linear Optical Behavior. *Chem. Phys. Lett.* **2022**, *803*, No. 139843.
(29) Malik, H.; Akhter, Z.; Shahbaz, M.; Yousuf, S.; Munawar, K. S.; Muhammad, S.; Qamar, S.; Abbas, A.; Ashfaq, M.; Ahmad, T. Synthesis, spectroscopic characterization, single crystal, theoretical investigation, and biological screenings of azo-based moieties. *J. Mol. Struct.* **2022**, *1270*, No. 133867.
(30) Khan, B. A.; Ashfaq, M.; Muhammad, S.; Munawar, K. S.; Tahir, M. N.; Al-Sehemi, A. G.; Alarfaji, S. S. Exploring Highly Functionalized Tetrahydropyridine as a Dual Inhibitor of Monoamine Oxidase A and B: Synthesis, Structural Analysis, Single Crystal XRD, Supramolecular Assembly Exploration by Hirshfeld Surface Analysis, and Computational Studies. *ACS Omega* **2022**, *7*, 29452−29464.
(31) Faihan, A. S.; Aziz, N. M.; Ashfaq, M.; Hassan, W. M. I.; Al-Jibori, S. A.; Al-Janabi, A. S.; Tahir, M. N.; Al-barwari, A. S. M. O. Synthesis, characterization, and x-ray crystallography of unexpected chloro-substitution on 1-(4-chlorophenyl)-3-phenylthiourea platinum(II) complex with tertiary phosphine ligand. *J. Mol. Struct.* **2022**, *1270*, No. 133985.
(32) Ali, A.; Khalid, M.; Ashfaq, M.; Malik, A. N.; Tahir, M. N.; Assiri, M. A.; Imran, M.; de AlcântaraMorais, S. F.; Braga, A. A. C. Preparation, QTAIM and Single-Crystal Exploration of the Pyrimethamine-Based Co-Crystal Salts with Substituted Benzoic Acids. *ChemistrySelect* **2022**, *7*, No. e202200349.
(33) Khalid; Ali, A.; Abid, S.; Tahir, M. N.; Khan, M. U.; Ashfaq, M.; Imran, M.; Ahmad, A. Facile Ultrasound-Based Synthesis, SC-XRD, DFT Exploration of the Substituted Acyl-Hydrazones: An Experimental and Theoretical Slant towards Supramolecular Chemistry. *ChemistrySelect* **2020**, *5*, 14844−14856.
(34) Khalid, M.; Ali, A.; Tariq, J.; Tahir, M. N.; Aliabad, H. A. R.; Hussain, I.; Ashfaq, M.; Khan, M. U. Stabilization of Supramolecular Assembly of N-Substituted Benzylidene Acetohydrazide Analogs by Non-Covalent Interactions: A Concise Experimental and Theoretical Approach. *ChemistrySelect* **2020**, *5*, 10618−10631.
(35) McKinnon, J. J.; Jayatilaka, D.; Spackman, M. A. Towards quantitative analysis of intermolecular interactions with Hirshfeld surfaces. *Chem. Commun.* **2007**, *37*, 3814−3816.
(36) Iqbal, Y.; Haroon, M.; Akhtar, T.; Ashfaq, M.; Tahir, M. N.; Rasheed, L.; Yousuf, M.; Zia, M. A. Synthesis, Spectroscopic Characterization, Single Crystal XRD, Hirshfeld Surface Analysis and Theoretical Studies (DFT) of 4-Adamantyl-(2-(substitutedbenzylidene) hydrazinyl) thiazoles. *J. Mol. Struct.* **2022**, *1267*, No. 133620.
(37) Kargar, H.; Fallah-Mehrjardi, M.; Behjatmanesh-Ardakani, R.; Bahadori, M.; Moghadam, M.; Ashfaq, M.; Munawar, K. S.; Tahir, M. N. Spectroscopic investigation, molecular structure, catalytic activity with computational studies of a novel Pd (II) complex incorporating unsymmetrical tetradentate Schiff base ligand. *Inorg. Chem. Commun.* **2022**, *142*, No. 109697.
(38) Kargar, H.; Ashfaq, M.; Fallah-Mehrjardi, M.; Behjatmanesh-Ardakani, R.; Munawar, K. S.; Tahir, M. N. Unsymmetrical Ni (II) Schiff base complex: Synthesis, spectral characterization, crystal structure analysis, Hirshfeld surface investigation, theoretical studies, and antibacterial activity. *J. Mol. Struct.* **2022**, *1265*, No. 133381.
(39) Jelsch, C.; Ejsmont, K.; Huder, L. The enrichment ratio of atomic contacts in crystals, an indicator derived from the Hirshfeld surface analysis. *IUCrJ* **2014**, *1*, 119−128.
(40) Askerov, R. K.; Ashfaq, M.; Chipinsky, E. V.; Osmanov, V. K.; Tahir, M. N.; Baranov, E. V.; Fukin, G. K.; Khrustalev, V. N.; Nazarov, R. H.; Borisova, G. N.; Matsulevich, Z. V.; Maharramov, A. M.; Borisov, A. V. Synthesis, crystal structure, exploration of the supramolecular assembly through Hirshfeld surface analysis and bactericidal activity of the cadmium organometallic complexes obtained from the heterocyclic ligand. *Results Chem.* **2022**, *4*, No. 100600.
(41) Ali, A.; Ashfaq, M.; Din, Z. U.; Ibrahim, M.; Khalid, M.; Assiri, M. A.; Riaz, A.; Tahir, M. N.; Rodrigues-Filho, E.; Imran, M.; Kuznetsov, A. Synthesis, Structural, and Intriguing Electronic Properties of Symmetrical Bis-Aryl-α,β-Unsaturated Ketone Derivatives. *ACS Omega* **2022**, *7*, 39294−39309.
(42) Turner, M. J.; McKinnon, J. J.; Jayatilaka, D.; Spackman, M. A. Visualisation and characterisation of voids in crystalline materials. *CrystEngComm* **2011**, *13*, 1804−1813.
(43) Ashfaq, M.; Khalid, M.; Tahir, M. N.; Ali, A.; Arshad, M. N.; Asiri, A. M. Synthesis of Crystalline Fluoro-Functionalized Imines, Single Crystal Investigation, Hirshfeld Surface Analysis, and Theoretical Exploration. *ACS Omega* **2022**, *7*, 9867−9878.
(44) Kargar, H.; Ashfaq, M.; Fallah-Mehrjardi, M.; Behjatmanesh-Ardakani, R.; Munawar, K. S.; Tahir, M. N. Synthesis, characterization, SC-XRD, HSA and DFT study of a novel copper (I) iodide complex with 2-(thiophen-2-yl)-4, 5-dihydro-1H-imidazole ligand: An

https://doi.org/10.1021/acsomega.2c07686
ACS Omega 2023, 8, 8530−8540

experimental and theoretical approach. *J. Mol. Struct.* **2022**, *1253*, No. 132264.
(45) Ashfaq, M.; Tahir, M. N.; Muhammad, S.; Munawar, K. S.; Ali, A.; Bogdanov, G.; Alarfaji, S. S. Single-Crystal Investigation, Hirshfeld Surface Analysis, and DFT Study of Third-Order NLO Properties of Unsymmetrical Acyl Thiourea Derivatives. *ACS Omega* **2021**, *6*, 31211−31225.
(46) Muhammad, N.; Khan, I. N.; Ali, Z.; Ibrahim, M.; Shujah, S.; Ali, S.; Ikram, M.; Rehman, S.; Khan, G. S.; Wadood, A. Synthesis, characterization, antioxidant, antileishmanial, anticancer, DNA and theoretical SARS-CoV-2 interaction studies of copper (II) carboxylate complexes. *J. Mol. Struct.* **2022**, *1253*, 132308.
(47) Frisch, A., *gaussian 09W Reference*. Wallingford, USA, *25p* 2009, 470.
(48) Champagne, B.; Perpète, E. A.; Jacquemin, D.; Van Gisbergen, S. J.; Baerends, E.-J.; Soubra-Ghaoui, C.; Robins, K. A.; Kirtman, B. Assessment of conventional density functional schemes for computing the dipole moment and (hyper) polarizabilities of push− pull π-conjugated systems. *J. Phys. Chem. A* **2000**, *104*, 4755−4763.
(49) Muhammad, S.; Shehzad, R. A.; Iqbal, J.; Al-Sehemi, A. G.; Saravanabhavan, M.; Khalid, M. Benchmark study of the linear and nonlinear optical polarizabilities in proto-type NLO molecule of para-nitroaniline. *J. Theor. Comput. Chem.* **2019**, *18*, 1950030.
(50) Dennington, R.; Keith, T. A.; Millam, J. M. *GaussView, Version 6.1.1*, Semichem Inc., Shawnee Mission, KS., 2019.
(51) Muhammad, S.; Xu, H.; Janjua, M. R. S. A.; Su, Z.; Nadeem, M. Quantum chemical study of benzimidazole derivatives to tune the second-order nonlinear optical molecular switching by proton abstraction. *Phys. Chem. Chem. Phys.* **2010**, *12*, 4791−4799.
(52) Muhammad, S.; Xu, H.; Su, Z.; Fukuda, K.; Kishi, R.; Shigeta, Y.; Nakano, M. A new type of organic−inorganic hybrid NLO-phore with large off-diagonal first hyperpolarizability tensors: a two-dimensional approach. *Dalton Trans.* **2013**, *42*, 15053−15062.
(53) Muhammad, S. Quantum chemical design of triple hybrid organic, inorganic and organometallic materials: An efficient two-dimensional second-order nonlinear optical material. *Mater. Chem. Phys.* **2018**, *220*, 286−292.
(54) Muhammad, S.; Nakano, M.; Al-Sehemi, A. G.; Irfan, A.; Chaudhry, A. R.; Tonami, T.; Ito, S.; Kishi, R.; Kitagawa, Y. Exploring the novel donor-nanotube archetype as an efficient third-order nonlinear optical material: asymmetric open-shell carbon nanotubes. *Nanoscale* **2018**, *10*, 16499−16507.
(55) Mohan, B.; Choudhary, M.; Muhammad, S.; Das, N.; Singh, K.; Jana, A.; Bharti, S.; Algarni, H.; Al-Sehemi, A. G.; Kumar, S. Synthesis, characterizations, crystal structures, and theoretical studies of copper(II) and nickel(II) coordination complexes. *J. Coord. Chem.* **2020**, *73*, 1256−1279.
(56) Mohan, B.; Choudhary, M.; Kumar, G.; Muhammad, S.; Das, N.; Singh, K.; Al-Sehemi, A. G.; Kumar, S. An experimental and computational study of pyrimidine based bis-uracil derivatives as efficient candidates for optical, nonlinear optical, and drug discovery applications. *Synth. Commun.* **2020**, *50*, 2199−2225.
(57) Mohan, B.; Choudhary, M.; Bharti, S.; Jana, A.; Das, N.; Muhammad, S.; Al-Sehemi, A. G.; Kumar, S. Syntheses, characterizations, crystal structures and efficient NLO applications of new organic compounds bearing 2-methoxy-4-nitrobenzeneamine moiety and copper (II) complex of (E)-N ′-(3, 5-dichloro-2-hydroxybenzylidene) benzohydrazide. *J. Mol. Struct.* **2019**, *1190*, 54−67.
(58) Munawar, K. S.; Ali, S.; Muhammad, S.; Ashfaq, M.; Abbas, S. M.; Tahir, M. N.; Siddeeg, S. M.; Ahmed, G. Synthesis, crystal structure, Hirshfeld surface analysis, DNA binding, optical and nonlinear optical properties of Schiff bases derived from o-aminophenol. *J. Mol. Struct.* **2022**, *1274*, 134427.
(59) Shahzad Munawar, K.; Ali, S.; Ashfaq, M.; Nawaz Tahir, M.; Muhammad, S.; Alarfaji, S. S.; Ahmed, G.; Al-Sehemi, A. G. Synthesis, Characterization, Crystal Structure and Computational Study of Third-Order NLO Properties of Schiff bases. *ChemistrySelect* **2022**, *7*, No. e202203015.
(60) Madni, M.; Ahmed, M. N.; Abbasi, G.; Hameed, S.; Ibrahim, M. A. A.; Tahir, M. N.; Ashfaq, M.; Gil, D. M.; Gomila, R. M.; Frontera, A. Synthesis and X-ray Characterization of 4,5-Dihydropyrazolyl-Thiazoles Bearing a Coumarin Moiety: On the Importance of Antiparallel π-Stacking. *ChemistrySelect* **2022**, *7*, No. e202202287.
(61) Sheldrick, G. M. SHELXT: Integrating space group determination and structure solution. *Acta Crystallogr., Sect. A: Found. Adv* **2014**, *70*, C1437.
(62) Sheldrick, G. M. Crystal structure refinement with SHELXL. *Acta Crystallogr. C Struct. Chem.* **2015**, *71*, 3−8.
(63) Farrugia, L. J. WinGX and ORTEP for Windows: an update. *J. Appl. Crystallogr.* **2012**, *45*, 849−854.
(64) Spek, A. L. Structure validation in chemical crystallography. *Acta Crystallogr. D Biol. Crystallogr.* **2009**, *65*, 148−155.
(65) Macrae, C. F.; Sovago, I.; Cottrell, S. J.; Galek, P. T.; McCabe, P.; Pidcock, E.; Platings, M.; Shields, G. P.; Stevens, J. S.; Towler, M.; Wood, P. A. Mercury 4.0: From visualization to analysis, design and prediction. *J. Appl. Crystallogr.* **2020**, *53*, 226−235.

https://doi.org/10.1021/acsomega.2c07686
ACS Omega 2023, 8, 8530−8540